Proc. Natl. Acad. Sci. USA
Vol. 92, pp. 574–578, January 1995
Biophysics

The force generated by a single kinesin molecule against an elastic load

EDGAR MEYHÖFER* AND JONATHON HOWARD†

Department of Physiology and Biophysics, SJ-40, University of Washington, Seattle, WA 98195

Communicated by Bertil Hille, University of Washington, Seattle, WA, October 18, 1994 (received for review September 21, 1994)

ABSTRACT **To probe the mechanism by which the motor protein kinesin moves along microtubules, we have developed a highly sensitive technique for measuring the force exerted by a single motor molecule. In this technique, one end of a microtubule is attached to the tip of a flexible glass fiber of calibrated stiffness. The other end of the microtubule makes contact with a surface sparsely coated with kinesin. By imaging the tip of the glass fiber on a photodiode detector, displacement of the microtubule by kinesin through as little as 1 nm can be detected and forces as small as 1 pN resolved. Using this force-fiber apparatus we have characterized the mechanical output of this molecular motor. The speed at which a molecule of kinesin moved along the surface of a microtubule decreased linearly as the elastic force was increased. The force required to stop a single kinesin molecule was 5.4 ± 1.0 pN (mean ± SD; n = 16), independent of the stiffness of the fiber, the damping from the fluid, and whether the ATP concentration was high or low.**

A motor protein, such as the actin-based motor myosin or the microtubule-based motors dynein and kinesin, is an enzyme that converts the free energy contained in the γ-phosphate bond of ATP into mechanical work used to power cellular motility. As it hydrolyzes a molecule of ATP, the motor protein is thought to undergo a series of conformational changes. One of these structural transitions is assumed to occur while the motor is attached to the filament and to introduce strain into the protein—according to this model, the relief of the strain is the driving force for the motion of the motor with respect to the filament. In the standard models (1–3), it is thought that during each cycle of ATP hydrolysis, the motor moves a small distance (≤ the size of the motor) toward the next equivalent binding site on the surface of the filament. Because the net motion is always in one direction, the subsequent rebinding of the motor to the filament is biased in one direction and directed movement ensues. Since myosin, dynein, and kinesin have structural and biochemical similarities, it is thought that they all work by a similar general mechanism. We are interested in understanding this mechanism.

Kinesin has proved to be a good model for studying force generation. First, it is the smallest motor. Kinesin's motor domain is ≈10 nm long and contains only 340 amino acids (4–6). Thus kinesin's motor domain, also called a "head," is about one-third the molecular weight of myosin's motor domain and one-tenth that of dynein's. A second advantage of kinesin is its simple subunit structure; the minimal active motor molecule is a homodimer, with each subunit contributing one motor domain (7–9). A third advantage is that a single kinesin molecule is capable of motility *in vitro*. In the microtubule gliding assay, a single molecule of kinesin fixed to a plane glass surface can move a microtubule through several micrometers before letting the microtubule go (10). In the bead assay, a single molecule fixed to a glass sphere can move 1–2 μm along a fixed microtubule before the motor dissociates from the microtubule (11). Myosin (and probably dynein) requires dozens of motors for continuous filament movement (12); this makes motility more difficult to study.

Single-motor assays, together with biochemical measurements, have provided much information concerning kinesin's energy-transducing mechanism. There is only one site per tubulin dimer for a kinesin head to bind to a microtubule (6). The tubulin dimers form protofilaments that run parallel to the axis of the microtubule; because kinesin follows a path parallel to the protofilaments (13), the distance between kinesin's consecutive binding sites, the step size, is most likely 8 nm (14), the spacing of the dimers along the protofilament. At high ATP concentration, kinesin moves at a rate of 500–1000 nm/s. With one step per ATP, this speed requires an ATP cycling rate of ≈50 per s per head; such high rates have been measured for kinesin heads produced by proteolysis (15) or mutagenesis (6), consistent with kinesin stepping 8 nm per ATP hydrolyzed.

Because the movement of a motor with respect to its filament ensues from a mechanical change within the motor, an understanding of the energy transduction process requires the definition of the forces originating within the motor. As an initial step toward such a description, several laboratories have measured the effect of external loads on the motion of kinesin (16–19) and myosin (20, 21), although with variable results. To accurately define the dependence of kinesin's motion on force, we have developed a very sensitive apparatus that permits the measurement of force and displacement with molecular resolution. Using this force-fiber apparatus we have measured the elastic force required to stall a single motor.

MATERIALS AND METHODS

General Methods. Kinesin and tubulin were purified from bovine brain (22). All reagents were obtained from Sigma unless otherwise stated. Some tubulin was labeled with ≈1 tetramethylrhodamine per dimer (23). Detailed methods for performing and analyzing standard motility assays—constructing flow cells, cleaning glass surfaces, adsorbing kinesin to glass surfaces, imaging fluorescent microtubules, video taping, and analyzing microtubule speeds—are described by Howard *et al.* (22). All experiments were done in standard buffer solution (80 mM potassium Pipes/1 mM EGTA/2 mM $MgCl_2$, pH 6.9 with KOH) at 25 ± 1°C.

Biotinylation of Microtubules. Equimolar rhodamine-labeled and unlabeled tubulin were polymerized in 2-(*N*-morpholino)ethanesulfonic acid buffer under conditions that favor the formation of 13-protofilament microtubules (13). Microtubules stabilized by addition of taxol to 10 μM were then incubated with the succinimidyl ester of 6-{[6-((biotinoyl)amino)hexanoyl]-amino}hexanoic acid (Molecular Probes) in 12-fold molar excess over tubulin at 37°C for 20 min. The reaction was quenched with

The publication costs of this article were defrayed in part by page charge payment. This article must therefore be hereby marked "*advertisement*" in accordance with 18 U.S.C. §1734 solely to indicate this fact.

*Present address: Abteilung für Klinische Physiologie, Medizinische Hochschule Hannover, 30623 Hannover, Germany.
†To whom reprint requests should be addressed.

a 10-fold excess of potassium glutamate over the biotin for an additional 5 min. Excess biotinylation reagents were then removed by two cycles of centrifugation. Control experiments showed that biotinylated microtubules moved at the same speed in the gliding assay (802 ± 26 nm/s) as unbiotinylated microtubules (841 ± 34 nm/s). We think that it is unlikely that biotinylation alters the single-motor force because experiments using the buckling assay (24) in which kinesin interacts with nonbiotinylated microtubules give similar forces (within ≈50%) to those measured here using the force-fiber apparatus.

Experimental Chamber. Force-fiber measurements were made in an open chamber constructed by adhering with high vacuum grease an annulus of Plexiglas 3 mm wide, 0.6 mm high, and with an inner diameter of 19 mm to a glass microscope slide. To facilitate the interaction between the rigid microtubule and the planar surface of the chamber, the glass slide was spangled with glass spheres (Fig. 1) of 2.5 μm diameter (Bangs Laboratories, Carmel, IN) by pretreating the glass slide with 2 μl of 0.1% spheres in distilled water and drying. Casein (100 μl; 200 μg/ml) in standard buffer was added to the chamber in order to pretreat the surfaces for single-motor assays (10, 11). This pretreatment had the added advantage that it rigidly affixed the glass spheres to the surface; the beads underwent no detectable Brownian motion (<1-nm rms over a 1-kHz bandwidth) and withstood forces in excess of 100 pN without dislodging. The chamber was then augmented with 100 μl of standard buffer solution containing kinesin diluted to 38–76 ng/ml for high ATP assays or to 12 ng/ml for low ATP assays. Assuming 100% adsorption to the surfaces, these concentrations correspond to kinesin densities of 16–32 or 5 per μm^2, respectively. The experimental chamber was then filled by addition of another 400 μl of standard buffer solution containing 100 ng of biotin-labeled microtubules per ml, 10 μM taxol, 100 μg of casein per ml, and ATP to give the stated concentration.

Attachment of Microtubules to the Force Fibers via a Biotin-Streptavidin Linkage. Glass fibers (100–200 μm long and ≈0.5 μm diameter) were constructed according to Howard and Hudspeth (25). The tip of each fiber was first dipped into a solution containing 0.15 mg of biotinylated bovine serum albumin (BSA) per ml (8–12 biotins per molecule of BSA; Pierce), washed twice in standard buffer, then dipped into a solution containing 0.1 mg of streptavidin per ml (Molecular Probes), and washed twice more before insertion into the chamber. To attach a microtubule to the tip of a fiber as shown in Fig. 1, the microscope stage was moved so that the microtubule in solution moved toward the tip of the force fiber. When the microtubule touched the tip of the fiber, a strong bond was formed about half the time; this bond could withstand forces up to 100 pN as demonstrated in earlier experiments in which the density of kinesin was much higher and the motion was due to many motors.

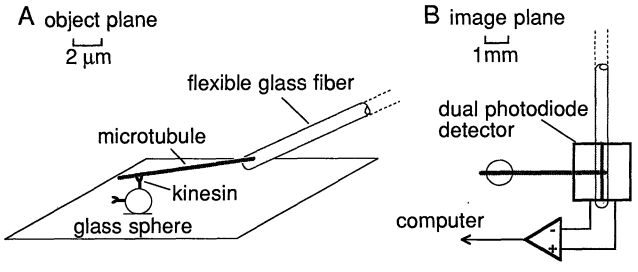

FIG. 1. Force-fiber technique. To measure forces generated by the motor protein kinesin, a microtubule attached to the tip of a flexible glass fiber is lowered to the surface of a kinesin-coated glass sphere. Magnified image of the tip of the fiber is projected onto a dual photodiode detector; the differential output is proportional to the position of the fiber and therefore to the attached microtubule.

Photodiode Detector. The tip of the fiber was magnified 390 times using a Diastar upright microscope (Leica, Deerfield, IL) and the dark-field image [Nikon; condenser numerical aperture (n.a.) 1.2–1.4; Zeiss ×40; 0.75-n.a. water immersion objective] was projected onto a dual photodiode detector (EG&G, Salem, MA) mounted on an *x–y* stage (type 401; Newport, Fountain Valley, CA) bolted to a vibration isolation table (Newport) (Fig. 1). The photocurrents were converted to voltages using 200-MΩ feedback resistors and low-noise operational amplifiers (OPA 627 AM; Burr Brown, Tucson, AZ), giving a bandwidth of ≈8 kHz. The difference in photocurrents between the detectors was proportional to the position of the fiber in the object plane up to displacements equal to the optical diameter of the fiber (≈0.5 μm). The displacement sensitivity was periodically calibrated by mounting the detector on a piezoelectric bimorph and driving the bimorph (under computer control) through a known distance in a direction perpendicular to the long axis of the detector's elements—this motion is equivalent to a smaller motion in the object plane (≈30 nm). The accuracy in the displacement, limited by errors in measurement of the magnification and of the bimorph displacement, was better than 2%.

Data Acquisition and Analysis. The voltages of the two photodiode channels were filtered at 1000 Hz using 4-pole Bessel filters (Ithaco, Ithaca, NY), amplified (Tektronix), and sampled to a personal computer at 4 kHz using a data acquisition board (National Instruments, Austin, TX). Data were transferred to a Macintosh computer for off-line analysis using a commercial software package (Igor, Lake Oswego, OR).

Calibration of Force Fibers. The stiffness of each fiber was calibrated by measuring its Brownian motion using the photodiode detector. This procedure, which has been checked for accuracy against other calibration techniques (25), has two advantages: it can be done *in situ* and it provides the time constant of the fiber. The fiber was positioned several micrometers above the surface, its tip was imaged on the photodetector, and the tip's thermal motion was recorded (Fig. 2*A*). A one-sided power spectrum was computed for each of 16 200-ms-long traces and a Lorentzian, $P(f)$, was fit by least squares to the average of the 16 spectra:

$$P(f) = 4\gamma k_B T \kappa_f^{-2}(1 + (2\pi\tau f)^2)^{-1},$$

where k_B is the Boltzmann constant, T is absolute temperature, κ_f is the stiffness of the fiber, γ is the damping, and τ (= γ/κ_f) is the time constant (Fig. 2*B*). The time constants varied between 0.33 and 5.7 ms.

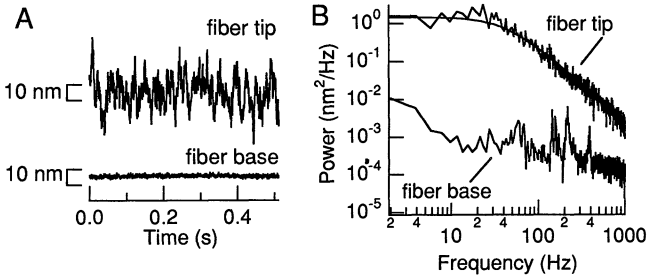

FIG. 2. Calibration of the fiber's stiffness. (*A*) Tip of a free fiber displayed a large thermally driven fluctuation with rms amplitude of ≈10 nm over the 1-kHz bandwidth of the recording. For comparison, the fluctuation measured at the base of the fiber had an amplitude of 0.64 nm, which corresponded to the noise floor of the apparatus. (*B*) Average, one-sided power spectra calculated from 8 traces like the ones shown in *A*. To estimate the fiber's stiffness, a Lorentzian (see text) was fitted to the spectrum. This fiber had a stiffness of 0.043 pN/nm, a time constant of 3.8 ms, and a damping coefficient of 0.16 μN·s/m.

Uncertainty in Force Measurements. There were three main sources of uncertainty that led to a systematic error in the force measurement of ≈10%. First, the maximum uncertainty associated with the fitting procedure was estimated to be ≈5%. Second, the site of attachment of the microtubule to the glass fiber differed slightly from the site on the fiber imaged onto the photodetector; the estimated maximum uncertainty was <7.5%. Third, the microtubule was neither exactly perpendicular to the glass fiber nor exactly parallel to the object plane. The total angular deviation was <30° so that the uncertainty should be <13% [1 − cos(30°)]. We estimated the systematic SEM as half the sum of the above uncertainties.

Measurement of the Speed–Force Curves. To determine the relation between speed and force, 2–11 displacement-time events made with the same fiber (such as the three shown in Fig. 3) were averaged (Fig. 4 *Insets*). A continuous, piecewise linear function comprising 10–20 segments was then fitted to the averaged time course by least squares. The speed was calculated as the slope of each segment and was plotted against the average force calculated as the mean displacement of each segment times the fiber stiffness.

Dependence of Maximum Force on ATP Concentration. In the simplest models (3, 19), the speed, v, in a single motor assay should be given by

$$v(F, [\mathrm{ATP}]) = \varepsilon dV = \varepsilon(F)d\frac{V_{\max}(F)[\mathrm{ATP}]}{K_m(F) + [\mathrm{ATP}]},$$

where d is the step size, ε is a coupling efficiency that is presumed to depend on the load but not the ATP concentration, V is the ATP cycling rate, and V_{max} and K_m are the Michaelis–Menten constants (26) that depend on the elementary rate constants (which in turn may depend on strain and load). This model is supported by experiments at low load—the dependence on the ATP concentration of kinesin's ATPase rate in solution (6) and kinesin's speed in the gliding assay (10) both follow this equation. In this paper, we found that the speed decreased approximately linearly as the force increased and that a similar maximum force was obtained at high (670 μM) and low (1.5 μM) ATP concentrations. In other words, we found that $v(F, 670\ \mu M)/v(F, 1.5\ \mu M) \approx$ constant (≈20). Substitution of the above equation shows that K_m (≈28 μM) must be independent of the load.

RESULTS

Force-Fiber Apparatus. In a force-fiber measurement from a kinesin molecule, a microtubule was attached perpendicularly to the tip of a flexible, horizontally mounted glass fiber (Fig. 1). The attachment was mediated via biotin that was covalently coupled to the microtubule and streptavidin that was adsorbed to the glass fiber. The base of the glass fiber was moved vertically with a hydraulic micromanipulator so that the distal end of the microtubule touched the top surface of a 2.5-μm-diameter glass sphere attached to the chamber bottom. The surfaces of the chamber had previously been sparsely coated with kinesin at a density of <30 per μm², low enough that the motility ought to be due to single motors (10, 11). After positioning the microtubule near the bead, the tip of the fiber was imaged onto the photodiode detector, which could measure the tip's position with a precision of ≈1-nm rms over the 1-kHz bandwidth of the recordings (Fig. 2).

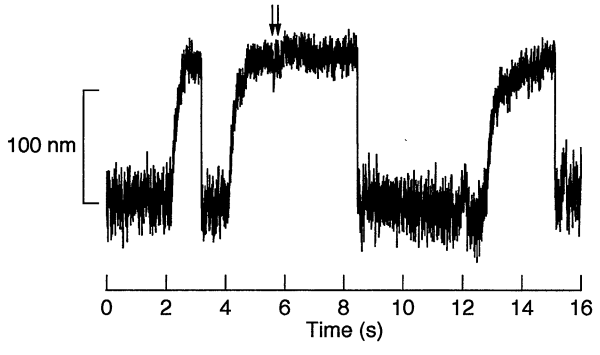

FIG. 3. Single kinesin molecule pulling a microtubule attached to a force fiber. Since the motor is fixed to the surface, the position of the fiber is equal to the distance moved by the motor relative to the microtubule. Fiber used here is the same as that shown in Fig. 2; its stiffness was 0.043 pN/nm, and the ATP concentration was 670 μM ATP. Arrows show small slips.

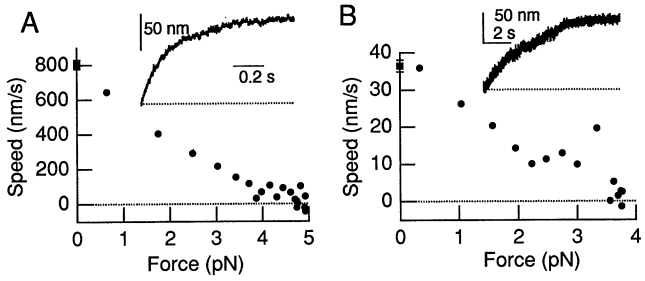

FIG. 4. Dependence of speed on elastic restoring force at high ATP concentration (*A*, [ATP] = 670 μM, κ_f = 0.043 pN/nm) and at low ATP concentration (*B*, [ATP] ≈ 1.5 μM, κ_f = 0.034 pN/nm). (*Insets*) Average time courses from which the speed–force curves were calculated as described. Squares correspond to the gliding speed measured in a flow cell under identical conditions.

Single-Motor Recordings. In ≈10% of the trials performed in the presence of ATP, the photodiode signal indicated that a motor was interacting with the microtubule. In about half the moving events, the motor pulled on the microtubule; since kinesin always moves toward the plus end of the microtubule the pulling is consistent with the microtubule's plus or fast-growing end being attached to the glass fiber. In the other 50% of the moving events, the motor pushed the microtubule toward the fiber and the microtubule often buckled; this is consistent with the microtubule being attached to the fiber at its minus end. Because this behavior was more complex it was not further studied.

Fig. 3 shows a kinesin molecule repeatedly pulling on a microtubule. Initially the microtubule was free, and the very soft glass fiber (43 μN/m = 0.043 pN/nm) underwent Brownian motion with a peak-to-peak amplitude of ≈60 nm. After a few seconds, the motor latched on and started pulling the microtubule, deflecting the fiber. Pari passu with the movement of the fiber there was a modest decrease in the fluctuations, indicating that the stiffness of the motor was similar to or greater than that of the fiber. The motor pulled the fiber through 120 nm and maintained that level for about a second before letting go. The fiber then recoiled to its initial position and resumed the large fluctuations. The amplitude and correlation time of the fluctuations after the recoil were similar to those of the free fiber measured during the calibration procedure, and the time course of the recoil was well fit by an exponential with a time constant similar to that of the correlation time of the motion of the free fiber; thus, during these two phases of the recording the fiber was likely to be detached from the motor. After about a second the motor reengaged. The record shows 3 of 11 such interactions that occurred with this fiber. While the times between encounters and the times spent at the maximum displacement were variable, the rise time and the maximum displacement associated with each encounter were similar from event to event. This stereotyped behavior, together with several other arguments summarized in the *Discussion*, indicates that each interaction is most likely due to a single motor, probably the same motor in each case.

The elastic force, F, acting on the motor via the glass fiber and microtubule is

$$F = \kappa_f(x - x_0),$$

where κ_f is stiffness of the fiber calibrated from the thermal motion of the free fiber (Fig. 2), x is the displacement of the tip of the fiber to which the microtubule is attached, and x_0 is the displacement of the tip of the fiber measured when the fiber is free. The average maximum displacement of 120 ± 10 nm (mean ± SD; n = 11) for the motor of Fig. 3 corresponds to a maximum force of 5.2 ± 0.5 pN.

The Force–Speed Relation. As the motor pulled on the microtubule, the flexion of the glass fiber increased, the elastic force opposing the motion increased, and the speed of movement decreased until a displacement asymptote was reached. At high ATP concentration (670 μM), the speed decreased approximately linearly with increasing force until a maximum force of ≈5 pN was reached (Fig. 4*A*). A similar linear relation between speed and force was observed at low ATP concentrations (≈1.5 μM; Fig. 4*B*). A linear force–speed relation predicts that the time course of the approach to maximum displacement be exponential. This was observed in the averaged traces (Fig. 4 *Insets*). At both high and low ATP concentrations, the initial speed of movement was similar to the gliding speed measured in a flow cell using identical microtubules and conditions; for five motors for which sufficient data were obtained to accurately measure a force–speed curve, the initial speed estimated by linear extrapolation was 0.98 ± 0.11 (mean ± SE) of the gliding speed where the fiber stiffnesses ranged from 0.034 to 0.106 pN/nm.

Dependence of Force on [ATP], Stiffness, and Damping. Measurements were made with glass fibers whose stiffnesses ranged from 0.034 to 0.63 pN/nm. For each of 16 fibers, up to 21 interactions (such as the three shown in Fig. 3) were recorded. For the 12 force-fiber measurements made at high ATP concentration (670 μM), the maximum forces ranged from 4.0 ± 0.3 to 7.6 ± 0.8 (mean ± SE) pN and the average maximum force was 5.5 ± 1.1 (mean ± SD; n = 12) pN. The coefficient of variation (SD/mean) of 0.2 for this population is somewhat larger than expected from the measurement errors, which included the uncertainty in the individual measurements (0.02–0.1), the uncertainty in the fiber calibration, and the uncertainty due to the microtubules not being orthogonal to the optical axis (see *Materials and Methods*). Thus, there may be a small (≈0.1) variability in maximum force from fiber to fiber (and thus possibly from motor to motor). The maximum force was independent of the stiffness of the fiber (Fig. 5*A*) even though the maximum displacements ranged from 140 to only 8 nm. The maximum force was also independent of the hydrodynamic damping on the fibers (Fig. 5*B*).

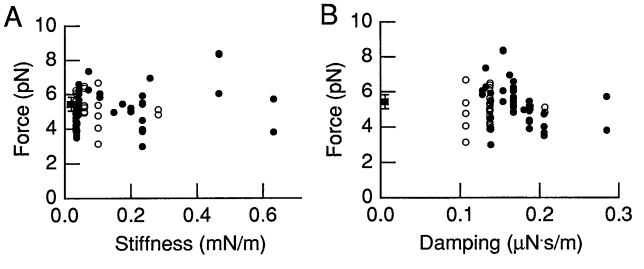

FIG. 5. Maximum force was independent of the stiffness (*A*) and the damping (*B*) of the fiber. Solid circles are high [ATP] (670 μM) and open circles are low [ATP] (≈1.5 to ≈3 μM). For this figure, the maximum force was measured from the amplitude of the recoil of the fiber from its maximum displacement to its free position. Each vertical cluster corresponds to several interactions of a motor with one fiber. Solid squares correspond to maximum force measured by Svoboda and Block (19) (average of forces at high and low ATP concentrations from their figure 9 *a* and *b*).

For the four force-fiber measurements at low ATP concentration (1.5 or 3 μM), the average maximum force was 5.1 ± 0.3 (mean ± SD) pN and there was no significant variability from motor to motor.

DISCUSSION

The Single-Motor Force. We used flexible glass fibers of calibrated stiffness to impose known loads on kinesin molecules fixed to a surface. When the density of kinesin on the surface was very low, we recorded stereotyped interactions between the motors and microtubules; the speed was initially high, close to the unloaded gliding speed, and decreased approximately linearly as a maximum force was approached. The maximum force was independent of the stiffness of the fiber, the hydrodynamic damping on the fiber, and the ATP concentration. The maximum force was 5.4 ± 1.0 (mean ± SD; n = 16) pN.

Three observations suggest that this force corresponds to the maximum force exerted by a single kinesin molecule. (*i*) The kinesin density on the surface was very low, comparable to or less than that used in earlier assays that display single-motor motility (10, 11). Making the generous assumptions that a motor can interact with a microtubule anywhere within a 60-nm radius and that kinesin adsorbs with 100% activity, we would expect that at most 0.5–3 kinesin molecules on the surface of the sphere could interact with the microtubule, and the actual number is probably much less. (*ii*) For a given fiber and bead, the interaction events were stereotyped; the rising phase of most interactions had a stereotyped time course, and the speed dropped to 0 at similar displacements. There was no evidence for different 0-speed displacement levels that might be expected if the interaction events were driven by a variable number of motors exerting a variable total force. (*iii*) Finally, a similar maximum force was obtained for all 16 fibers. This argues that the motions were driven by a functional motor of constant size. While it is formally possible that the functional motor is a small, constant-sized aggregate of native kinesin molecules (7, 22), this is unlikely since kinesin does not form aggregates in solution (7) or on EM grids (8, 9), and the formation of such aggregates is likely too slow at the very low concentrations of kinesin used to coat the surfaces (10). Thus, it is likely that the forces derive from single kinesin molecules.

Dependence of Force on Orientation. There was very little variability of maximum force from motor to motor (SD/mean ≈ 0.1). This is surprising given that the motors were adsorbed onto the beads' surfaces with random orientation. There are two possible explanations; either an incorrectly oriented motor cannot bind to and exert appreciable force against a microtubule or the relative angle between the orientation of the motor's site of attachment on the surface and the microtubule does not affect the force. The former possibility is unlikely; earlier studies showed that in the single-motor gliding assay kinesin can bind to and move a microtubule with a speed independent of the microtubule's orientation (27). Even though the earlier study was done under low loads (<1 pN) (18), when taken together with the present results it is likely that the maximum force generated by a motor is also independent of the microtubule's orientation. This is consistent with there being a highly flexible domain between kinesin's heads and kinesin's site of attachment to the surface (27).

The Stiffness of the Motor. The initial speed of movement was similar to the gliding speed measured in a flow cell using identical microtubules and conditions (ratio of 1.0 ± 0.1). This is perhaps not surprising since in the gliding assay the load on the motor is very small. The near equality of the initial speed measured in the force-fiber experiments and the speed measured in the almost-unloaded gliding assay implies that the motor is quite stiff; the ratio of the two speeds is expected to equal $\kappa_m/(\kappa_m + \kappa_f)$ and since the fibers used for these

observations had a mean stiffness (κ_f) of 0.05 pN/nm, we estimate that the motor stiffness (κ_m) must be at least 0.15 pN/nm. Similar reasoning implies that any series elasticity—for example, flexibility in the kinesin–glass or microtubule–fiber connections—must also be small. An appreciable motor stiffness is consistent with the reduction in amplitude of the thermally driven fluctuation of the glass fiber associated with the attachment of the motor to the microtubule (Fig. 3). If the noise recorded during the high-force plateau were solely due to the thermal fluctuations of fiber and motor springs (total stiffness, $\kappa_m + \kappa_f$), then the stiffness of the motor in Fig. 3 would be 0.06 pN/nm, and the average motor stiffness (κ_m) would be 0.15 ± 0.09 pN/nm (mean ± SD; $n = 16$). The true stiffness is likely to be larger since the fluctuations could originate from transitions between conformational states. Our results differ from those of Svoboda *et al.* (14), who inferred a motor stiffness (the "bead-MT linkage") of only 0.03 pN/nm.

Comparison to Other Work. The single-motor force reported here is very close to that measured against a viscous load (4–5 pN) (18) and against an elastic force exerted by an optical trap (5–6 pN) (19). Earlier studies (16, 17) giving forces of 0.12 and 1.9 pN are almost certainly in error (28). The approximately linear relation between force and speed is consistent with linear curves measured by Hunt *et al.* (18) and Svoboda and Block (19) and is predicted by several models (3, 18).

Why Does the Load Slow Down the Motor? The slowing down of kinesin's motion at high force must be due to (*i*) a decrease in the rate that the motor moves forward while attached to the microtubule, (*ii*) an increase in the rate that the motor slips back while detached, or (*iii*) a combination of the two.

The finding that the same maximum force is attained at both high and low ATP concentrations is consistent with any of these possibilities. This finding, together with the observation that the shape of the speed–force curve is independent of ATP concentration, leads to the interesting conclusion that the K_m for ATP—the ATP concentration required for a half-maximal cycle rate—is likely to be independent of load (see *Materials and Methods*). While it is possible that both the K_m and the ATP cycle rate are independent of load as in the Leibler and Huse model (3, 19), it is also possible for the cycle rate to depend on the load while the K_m does not. For example, if either ATP hydrolysis or phosphate release were rate limiting, then a load-dependent slowing of either rate would not change K_m since in either case the K_m equals the dissociation constant of ATP from the protein (26). Both cases require that kinesin, unlike myosin, unbinds from its filament after hydrolysis.

The motor sometimes makes small slips at high load (Fig. 3, arrows; see also ref. 19). Is increased slippage sufficient to explain the reduction in speed at high force? According to the Leibler and Huse model (3), the maximum force exerted against an elastic load (F_{max}) should equal $\kappa_m d/(1 + t_D\kappa_m/\gamma)$, where t_D is the time during which the motor is detached from the filament, d is the step size, and γ is the hydrodynamic damping. This relation simply says that the speed drops to 0 when the distance moved in the attached part of the cycle ($d - F/\kappa_m$) equals the distance slipped during the detached part of the cycle ($t_D F/\gamma$). The finding that the maximum force is independent of damping (Fig. 5*B*) implies that $t_D\kappa_m/\gamma << 1$ over the range of damping coefficients in Fig. 5*B* and that $F_{max} = \kappa_m d$. Thus, the Leibler and Huse model predicts that $t_D << \gamma d/F_{max} \approx 8$ μs. Independent evidence supporting this conclusion—namely, that slippage during the detached state must be very small—is that the maximum force exerted against an elastic load is similar to the maximum force exerted against a viscous load (18) where there is no slippage at all. Thus, we conclude that the motor slows because the rate of forward progress while attached decreases; this may occur because the ATPase cycle rate decreases with increasing load [this would be analogous to the Fenn effect observed in muscle (29)], or, if the cycle rate is independent of load as in the Leibler and Huse model, because the fraction of the cycles during which a step is made decreases.

We thank Fred Gittes for illuminating discussions throughout the duration of this work and Sung Baek for purifying proteins and excellent technical support. We also thank Albert Gordon, Bryant Chase, Stanislas Leibler, Linda Wordeman, and members of the Howard laboratory for comments on the manuscript. Special thanks are given to Wayne Crill and the University of Washington for providing space and facilities necessary for these experiments. E.M. was supported by a fellowship from the American Heart Association, Washington Affiliate. J.H. was supported by the National Institutes of Health (Grant AR40593) and the Pew Charitable Trusts as a Pew Scholar in the Biomedical Sciences and the Human Frontier Science Program.

1. Huxley, H. E. (1969) *Science* **164,** 1356–1366.
2. Lymn, R. W. & Taylor, E. W. (1971) *Biochemistry* **10,** 4617–4624.
3. Leibler, S. & Huse, D. (1993) *J. Cell Biol.* **121,** 1357–1368.
4. Yang, J. T., Saxton, W. M., Stewart, R. J., Raff, E. C. & Goldstein, L. S. B. (1990) *Science* **249,** 42–47.
5. Stewart, R. J., Thaler, J. P. & Goldstein, L. S. B. (1993) *Proc. Natl. Acad. Sci. USA* **90,** 5209–5213.
6. Huang, T.-G. & Hackney, D. D. (1994) *J. Biol. Chem.* **269,** 16493–16501.
7. Bloom, G. S., Wagner, M. C., Pfister, K. K. & Brady, S. T. (1988) *Biochemistry* **27,** 3409–3416.
8. Hirokawa, N., Pfister, K. K., Yorifuji, H., Wagner, M. C., Brady, S. T. & Bloom, G. S. (1989) *Cell* **56,** 867–878.
9. Scholey, J. M., Heuser, J., Yang, J. T. & Goldstein, L. S. B. (1989) *Nature (London)* **338,** 355–357.
10. Howard, J., Hudspeth, A. J. & Vale, R. D. (1989) *Nature (London)* **342,** 154–158.
11. Block, S. M., Goldstein, L. S. B. & Schnapp, B. J. (1990) *Nature (London)* **348,** 348–352.
12. Uyeda, T. Q. P., Kron, S. J. & Spudich, J. A. (1990) *J. Mol. Biol.* **214,** 699–710.
13. Ray, S., Meyhöfer, E., Milligan, R. A. & Howard, J. (1993) *J. Cell Biol.* **121,** 1083–1093.
14. Svoboda, K., Schmidt, C. F., Schnapp, B. J. & Block, S. M. (1993) *Nature (London)* **256,** 721–727.
15. Kuznetsov, S. A., Vaisberg, Y. A., Rothwell, S. W., Murphy, D. B. & Gelfand, V. I. (1989) *J. Biol. Chem.* **264,** 589–595.
16. Kuo, S. C. & Sheetz, M. P. (1993) *Science* **260,** 232–234.
17. Hall, K., Cole, D. G., Yeh, Y., Scholey, J. M. & Baskin, R. J. (1993) *Nature (London)* **364,** 457–459.
18. Hunt, A. J., Gittes, F. & Howard, J. (1994) *Biophys. J.* **67,** 766–781.
19. Svoboda, K. & Block, S. M. (1994) *Cell* **77,** 773–784.
20. Ishijima, A., Harada, Y., Kojima, H., Funatsu, T., Higuchi, H. & Yanagida, T. (1994) *Biochem. Biophys. Res. Commun.* **199,** 1057–1063.
21. Finer, J. T., Simmons, R. M. & Spudich, J. A. (1994) *Nature (London)* **368,** 113–119.
22. Howard, J., Hunt, A. J. & Baek, S. (1993) *Methods Cell Biol.* **39,** 137–147.
23. Hyman, A., Drechsel, D., Kellogg, D., Salser, S., Sawin, K., Steffen, P., Wordeman, L. & Mitchison, T. (1991) *Methods Enzymol.* **196,** 478–485.
24. Gittes, F., Meyhöfer, E., Baek, S. & Howard, J. (1994) *Biophys. J.* **66,** A312 (abstr.).
25. Howard, J. & Hudspeth, A. J. (1988) *Neuron* **1,** 189–199.
26. Fersht, A. (1985) *Enzyme Structure and Mechanism* (Freeman, New York), 2nd Ed.
27. Hunt, A. J. & Howard, J. (1993) *Proc. Natl. Acad. Sci. USA* **90,** 11653–11657.
28. Howard, J. (1993) *Nature (London)* **364,** 390–391.
29. Bagshaw, C. R. (1993) *Muscle Contraction* (Chapman & Hall, New York), 2nd Ed.